# A new Ni-base superalloy: production-microstructure-properties correlation

G. Angella, A. Serafini, C. Malara, M. F. Brunella

The new nickel-base super alloy AF955® (UNS N09955) was developed by Foroni S.p.A. in response to the industrial need for a material that preserves the excellent properties of the precipitation hardened nickel-based superalloys, while also providing adequate resistance to hydrogen embrittlement. A wide mechanical and microstructure characterization of the new superalloy was carried out to rationalize the effects of the production route and different heat treatments of alloy AF955®. Mechanical properties were evaluated by Rockwell hardness and tensile tests. The microstructure was investigated by conventional Optical Microscopy (OM) and Scanning Electron Microscopy (SEM) with micro-chemical measurements with Energy Dispersion Spectroscopy (EDS) for a general and phase precipitation assessment, and by Transmission Electron Microscopy (TEM) for a quantitative characterization of the nanometric precipitation strengthening phases, namely gamma prime (γ′) phase and gamma double prime (γ′′) phase. Quantitative relationships between mechanical properties and strengthening precipitation phases, were obtained by using the Weakly Coupled Dislocation (WCD) model and the Strongly Coupled Dislocation (SCD) model. The WCD model for deformable particles resulted successful to correlate the quantitative microstructure results obtained through TEM with the yield strength of the new superalloy after two different heat treatments.

**KEYWORDS:** NICKEL-BASED SUPERALLOY, MECHANICAL PROPERTIES, STRAIN HARDENING, TEM, WEAKLY COUPLED DISLOCATION (WCD) MODEL.

## INTRODUCTION

Thanks to their excellent corrosion resistance and mechanical properties [1-3], the precipitation hardened nickel-base superalloys are paramount materials for oil and gas applications [4,5]. The new superalloy AF955® [6-9] was developed in response to an industrial need for materials that maintain the exceptional properties of the precipitation hardened (PH) nickel-base superalloys, while also comply on the new and more stringent microstructure requirements called out in the latest revision of the *American Petroleum Institute (API) Specification API 6ACRA* [9] as well as providing adequate resistance to hydrogen embrittlement. This required a wide mechanical and microstructure characterization to optimize the production route and post-forging heat treatments of the new superalloy AF955®.

AF955® contains chemical elements like Ti, Nb and Al that are expected to contribute to the alloy hardening through the precipitation of $Ni_3$(Al, Ti) gamma prime (γ′) and $Ni_3$Nb gamma double prime (γ′′) phases. The γ′ phase has an ordered L12 crystallographic structure with a pseudo-spherical/

Giuliano Angella
CNR-ICMATE Istituto di Chimica della Materia Condensata e di Tecnologie per l'Energia
giuliano.angella@cnr.it

Maria Francesca Brunella
Dipartimento di Chimica, Materiali e Ingegneria Chimica "Giulio Natta"
francesca.brunella@polimit.it

Carlo Malara
Foroni S.p.A.
carlo.malara@foronispa.com

Andrea Serafini
ST Microelectronics - Agrate Brianza (MB) – Italy
andrea_serafini@hotmail.com

cubical particle shape, and precipitates consistently with the face-centered-cubic (fcc) γ matrix, according to a cube-on-cube relationship (001)γ'||(001)γ and [100]γ'||[100]γ. The γ'' phase has a D022 body-centered-tetragonal structure with disc-shape particles coherent with the fcc γ matrix with the following orientation relationship: (001)γ''||{001}γ and [100]γ''||<100>γ. Both γ' and γ'' precipitates contribute significantly to the strength of nickel-base superalloys at different extents according to micro-mechanisms of interaction with dislocations motion. Physical properties, volume fractions and size of γ' and γ''precipitates (and so inter-particle distances) are key features in affecting the micro-mechanisms of interaction with dislocations motion strengths, and are determined by production route and post-forging heat treatments. To optimize the process production, a wide mechanical and microstructure characterization of the new nickel-base superalloy AF955® was needed and the results of this characterization are here reported. Mechanical properties were evaluated by Rockwell hardness and tensile tests. Investigations by conventional Optical Microscopy (OM) and Scanning Electron Microscopy (SEM) with micro-chemical measurements with Energy Dispersion Spectroscopy (EDS) were carried out for general assessment of the microstructure homogeneity of the forged work-piece and coarse precipitation in the superalloy after forging and heat treatment. For quantitative characterization of the nanometric strengthening precipitation phases, namely gamma prime (γ') and gamma double prime (γ'') phases, Transmission Electron Microscopy (TEM) was carried out on the superalloy after different heat treatments. The volume fractions of the strengthening precipitates were estimated through TEM imaging techniques [10,11]. Weakly Coupled Dislocation (WCD) and Strongly Coupled Dislocation (SCD) models were used to rationalise the yield strengths of the superalloy as a function of different heat treatments. The WCD model for deformable particles resulted successful to correlate the nanometric microstructure results of gamma prime (γ') and gamma double prime (γ'') phases with the strength of the new superalloy.

## MATERIAL AND EXPERIMENTALS

The chemical composition in %wt of alloy AF955® used in this study is reported in Table 1.

**Tab.1** - Chemical composition of alloy AF955® (%wt).

| Ni | Cr | Mo | Nb | Ti | Al | Si | Mn | C | P | S | Fe |
|---|---|---|---|---|---|---|---|---|---|---|---|
| 57.4 | 21.6 | 5.88 | 4.80 | 0.86 | 0.43 | 0.09 | 0.08 | 0.015 | 0.0086 | 0.0002 | 8.65 |

The alloy was produced by raw material melting in Electric Arc Furnace (EAF) of 70 tons capacity followed by melt refining via the Argon-Oxygen Decarburization (AOD) process, followed by re-melting through the consumable-electrode Vacuum Arc Re-melting (VAR) process. Two bars of 127 mm (5 in.) in diameter and about 6 m in length were forged from the same ingot and heat treated according to two different heat treatments, producing AF955® Gr. 3 and Gr. 3HS grades. The heat treatment of AF955® Gr. 3 consisted of solution annealing at 1060°C for 3 hours and 15 minutes followed by water quenching, followed by precipitation hardening at 746°C for 4 hours followed by air cooling. The heat treatment of AF955® Gr. 3HS consisted of the same heat treatment of AF955® Gr. 3 followed by the additional step of precipitation hardening at 621°C for 8 hours followed by air cooling.

For mechanical properties, Rockwell hardness tests were performed in accordance with ASTM E18 over the product cross-section, while room temperature tensile tests were carried out as per ASTM E8/E8M on specimens machined at mid radius of a bar prolongation of each tested product.

Microstructure examination was performed by conventional optical microscopy on specimens machined at center, mid radius and near surface of the cross-section of each tested product. The average grain size was determined according to ASTM E112 – comparison method and the grain size distribution was assessed as per ASTM E1181. For higher resolution microstructure investigations, Zeiss EVO 50 EP extended pressure Scanning Electron Microscope (SEM) and Oxford Inca 200 microanalysis system with Si(Li) windowless detector were used. Metallographic samples were observed in high vacuum condition at an accelerating voltage of 20 kV and probe current of 90 pA. TEM observations were carried out using a Philips CM 200 FEG electron microscope working at 200 kV acceleration voltage. Thin foils for TEM observations were prepared by grinding disk samples into foils with thickness of 80 μm followed by ion beam milling (GATAN DuoMill). The sizes of γ' and γ'' precipita-

tes for volume fractions calculations were determined with Dark Field (DF) TEM images through open source ImageJ software, after measurements of the thickness of samples in the DF TEM acquisition mode through Convergent Beam Electron Diffraction (CBED) technique.
Since γ′ and γ′′ presented overlapping reflections, various DF-TEM micrographs of the same area were collected under different DF conditions to discriminate between γ′and three types of possible γ′′ phases. Details of the acquisition procedure are reported in [10,11]. The volume fractions of γ′ and γ′′ evaluated in this study, considered the contribution of the precipitates oriented along the [100] and [010] axes.

## RESULTS

### *Mechanical properties*

Rockwell C-hardness (HRC) was determined at centre (C), mid radius (MR) and near the outer diameter surface (S) of the cross-section of each investigated product. Results of C-hardness measurements are given in Table 2.

**Tab.2** - ASTM E18 Rockwell C-hardness at centre (C), mid radius (MR) and near the outer diameter surface (S) of 127 mm diameter bars of AF955® superalloy.

| | Position | | |
|---|---|---|---|
| | ***C*** | ***MR*** | ***S*** |
| ***Gr. 3*** | 37 | 38 | 37 |
| ***Gr. 3HS*** | 40 | 40 | 39 |

Because variations in the thermo-mechanical conditions during forging occur, differences in grain size and precipitates morphology might occur [12,13] and, as a consequence, in the mechanical properties. The hardness variation over the product cross-section is 1 HRC maximum, indicating high degree of homogeneity of both Gr. 3 and Gr. 3HS products. However, the grade 3HS resulted always harder than the Gr. 3, suggesting that the additional heat treatment at 621°C for 8 hours was effective.
The stress-strain engineering flow curves upon ASTM E8/E8M tensile testing at mid radius of alloy AF955® in solution annealed condition (S.A.), and precipitation hardened conditions as per Gr. 3, and precipitation hardened condition as per Gr. 3HS are reported in Fig. 1. Results of Yield Strength at 0.2 % offset (YS), the Ultimate Tensile (UTS), and elongation to rupture ($e_R$) upon the aforementioned tensile testing are reported in Table 3. With respect to the S.A. condition, precipitation hardening as per Gr. 3 produced significant strengthening in AF955® together with an expected reduction of ductility, and the additional heat treatment at 621°C for 8 hours as per Gr. 3HS conferred an additional strength increase with a minimal ductility decrease.

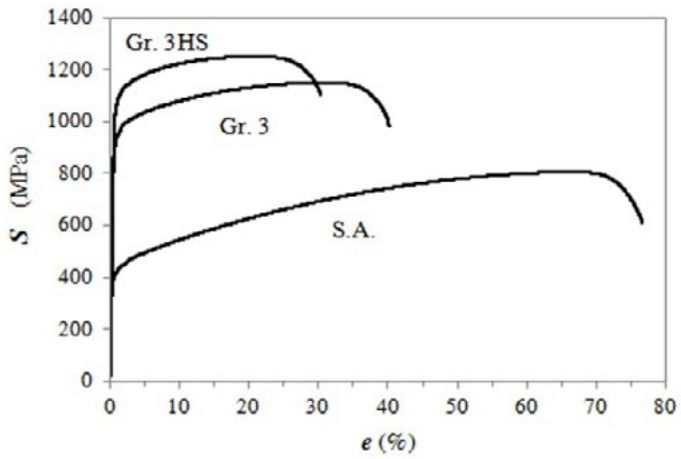


**Fig.1** - Engineering stress-strain curves upon ASTM E8/E8M tensile testing of alloyAF955® in the following conditions: solution annealed (S.A.), precipitation hardened as per Gr. 3 and precipitation hardened as per Gr. 3HS. Tensile specimens machined at mid radius of prolongations of: 152.4 mm diameter bar in the S.A. condition, 127 mm diameter bar in the Gr. 3 condition, 127 mm diameter bar in the Gr. 3HS condition.

**Tab.3** - Mechanical properties of alloyAF955® upon tensile testing curves in Figure 1.

| ***Heat Treatment*** | ***YS*** *(MPa)* | ***UTS*** *(MPa)* | $e_R$ *(%)* | ***AR*** *(%)* |
|---|---|---|---|---|
| ***S.A.*** *Bar diameter 152.4 mm* | 396.6 | 804.7 | 77 | 68 |
| ***Gr. 3*** *Bar Diameter 127 mm* | 910.8 | 1149.5 | 40 | 54 |
| ***Gr. 3HS*** *Bar Diameter 127 mm* | 1050.2 | 1249.8 | 30 | 50 |

### *Microstructure through OM and SEM*

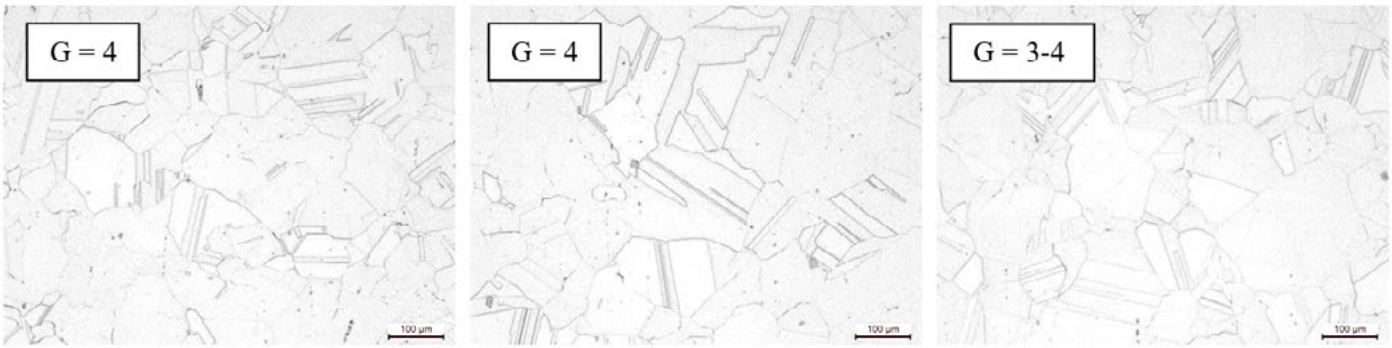


**Fig.2** - OM micrographs of grain structure of alloy AF955® - 127 mm diameter bar in the precipitation hardening condition as per Gr. 3: a) center; b) mid radius; c) near outer diameter surface. Grain size G was determined in accordance with ASTM E112 – comparison method.

Grain structure observations performed through conventional OM were carried out at different positions over the cross-section of alloy AF955® 127 mm diameter bars (centre, mid radius and near outer diameter surface). Grain size OM micrographs of grade Gr. 3 and grade Gr. 3HS of alloy AF955® are reported in Figs. 2 and 3, respectively. Grain size G was determined complying on ASTM E112 – comparison method. For both grades, the grain size G was No. 4 at center and mid radius locations, and slightly coarser up to No. 3-4 near outer diameter surface. The microstructure resulted therefore was essentially the same for both grades, very homogeneous over the entire product cross-section and no random or topological duplex grain size as determined and rated according to ASTM E1181 were observed.

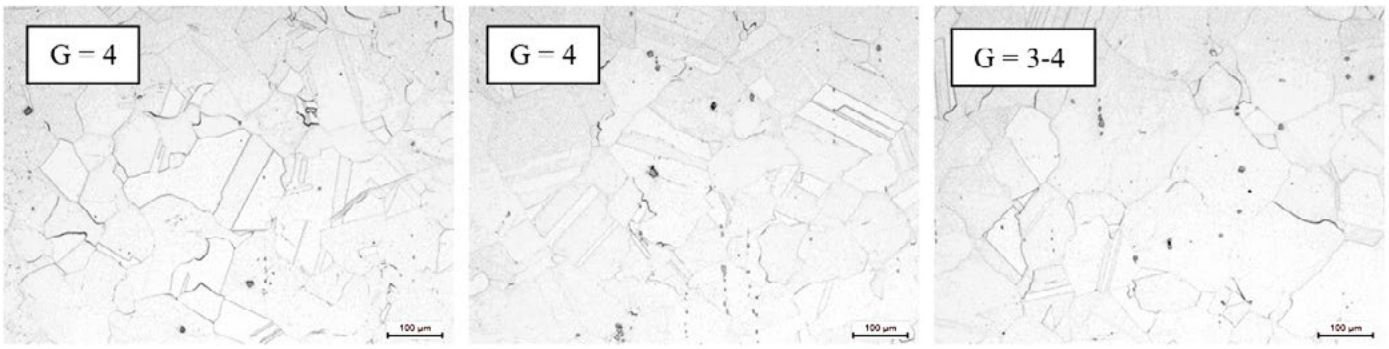


**Fig.3** - OM micrographs of grain structure of alloy AF955® - 127 mm diameter bar in the precipitation hardening condition as per Gr. 3HS: a) center; b) mid radius; c) near outer diameter surface. Grain size G was determined in accordance with ASTM E112 – comparison method.

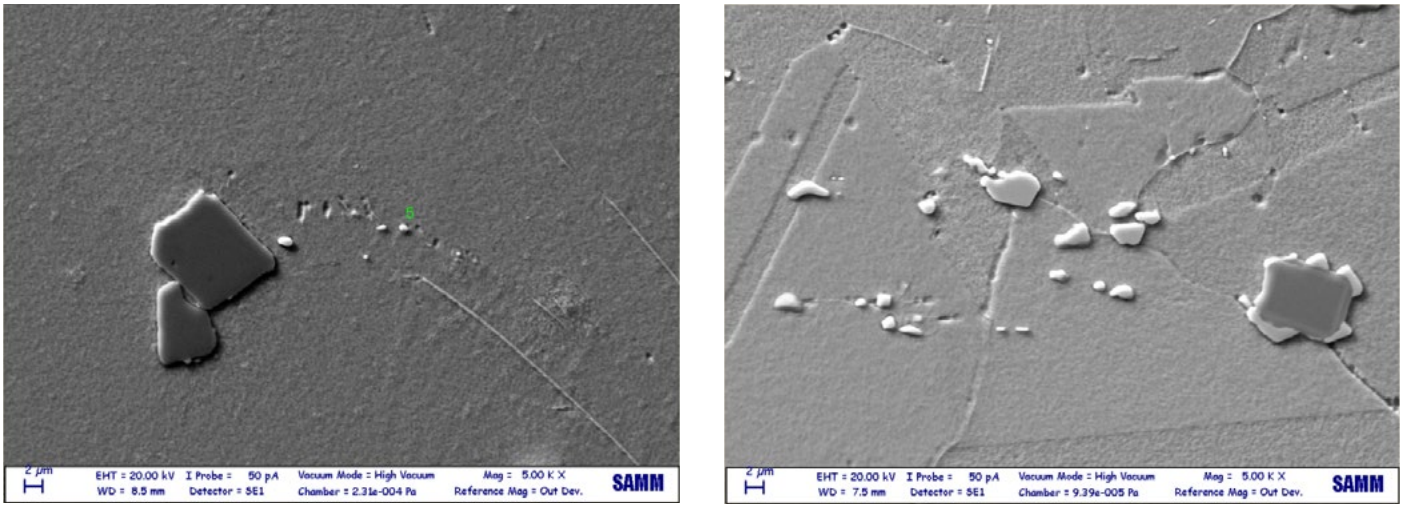


**Fig.4** - SEM micrographs (SEI) of coarse precipitates in alloy AF955® after heat treatment as per: a) Gr. 3 and b) Gr. 3HS.

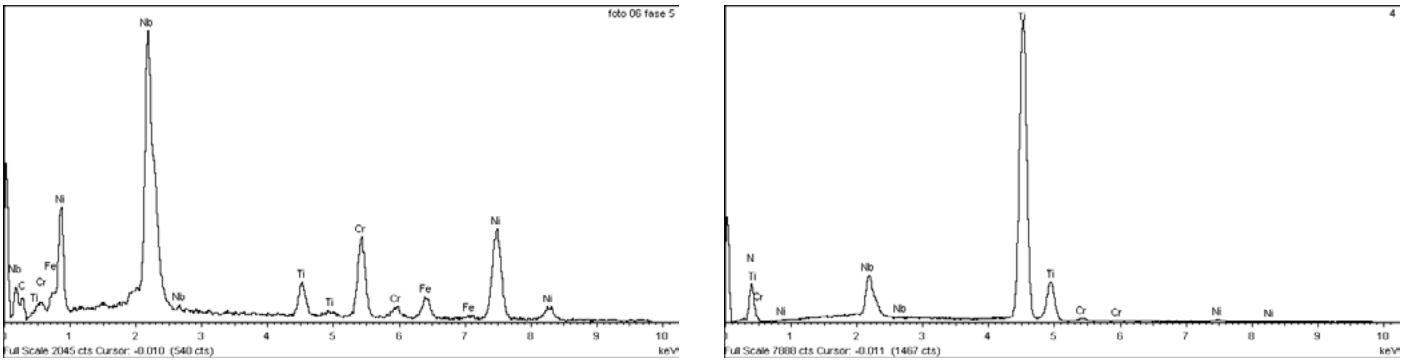


**Fig.5** - Typical EDS spectra from: a) small precipitates (bright) in micrographs reported in Figs. 4; b) coarse precipitates (grey) in micrographs reported in Figs. 4.

Observations of micrometric precipitates were performed in 127 mm diameter bars. Secondary Electron Imaging (SEI) SEM micrographs are reported in Fig. 4 for Gr. 3 and Gr. 3HS. Two different typologies of micrometric precipitates were found. Precipitates of prismatic shapes of about 10 µm diameter, and smaller irregular shape precipitates of 1-2 µm diameter. The two typologies of precipitates have different brightness, indicating that their chemical compositions could be significantly different. Secondary Electrons (SE) are insensitive to the atomic numbers (Z) of elements at the accelerating voltage of 20 kV, while Back-Scattered Electrons (BSE) are sensitive, having energy proportional to Z (and other physical parameters). However, BSEs can hit the SE detector contributing significantly to the SEI formation, showing different brightness with different precipitates. In Gr. 3HS the number of small precipitates seemed to be slightly increased because of the additional heat treatment compared to Gr. 3. In Fig. 5 typical EDS spectra from the two typologies of precipitates are reported, while the resulting chemical compositions are reported in Table 4. Even if the proper chemical composition determination of smaller micrometric precipitates through EDS on the SEM is hindered by the small size of the analyzed point, because of the X-rays coming from the adjacent matrix, some conclusions can be found by comparing the precipitate compositions with the matrix one. The chemical composition of the light grey precipitate with the EDS spectrum of Fig. 5a shows higher contents of C and Nb (also Ti is higher than in the matrix) than the matrix composition, revealing that the precipitates are Nb carbides or Nb-Ti-C. For the coarse precipitate of prismatic shape (Fig. 5b) N and Ti contents are higher (also Nb), revealing that the precipitates are Ti nitrides. Indeed, both these micrometric precipitates do not affect the strength of alloys, since their dimensions and characteristic inter-particle distances are by far larger than the nanometric Burgers vector modulus, one of the crystallographic parameters characterizing the interaction of dislocation motion with obstacles. However, these coarse precipitates could affect the ductility, particularly at high temperature, causing the occurrence of premature failure, which has been analysed later.

**Tab.4** - Chemical composition of precipitates determined by EDS analysis (% wt).

| Spectrum | C | N | Al | Si | Ti | Cr | Mn | Fe | Ni | Nb | Mo |
|---|---|---|---|---|---|---|---|---|---|---|---|
| **Fig. 5a** | 17.15 | - | 0.18 | 0.16 | 3.53 | 11.13 | 0.16 | 3.92 | 25.27 | 35.55 | 2.95 |
| **Fig. 5b** | 1.34 | 19.39 | - | - | 66.92 | 0.68 | - | 0.19 | 0.96 | 10.40 | 0.05 |
| **Matrix** | 3.26 | - | 0.46 | 0.08 | 0.94 | 21.84 | - | 7.83 | 54.75 | 4.83 | 6.07 |

***TEM-Microstructure***

Precipitates that affect significantly the strength of alloys, have dimensions and characteristic inter-particle distances comparable to the Burgers vector modulus of γ matrix, like for nanometric γ′ and γ′′ phase precipitates in nickel-base superalloys produced after proper heat treatments. TEM observations are needed for quantitative characterization of these nanometric precipitates. However, when γ′ and γ′′ precipitates are present, it is not possible to obtain Dark Field (DF) images of isolated γ′ particles, because all the γ′ phase reflections are superimposed to the γ′′ precipitates reflections [10,11,14]. This issue was solved by comparison of two DF images obtained after selecting firstly the γ′′ reflections and then the superimposed (γ′ + γ′′) reflections with the objective aperture. This technique [10,11,14] was used to acquire DF micrographs of AF955® samples after different heat treatments, and an example is reported in Fig. 6 for Gr. 3HS. In Fig. 6a, only γ′′ Selected Area Diffractions (SAD) reflections were selected and elongated γ′′ particles are visible in DF images. When γ′ + γ′′ SAD reflections are selected, also cubical γ′ precipitates appear, so discrimination could be done for quantitative precipitate measurements.

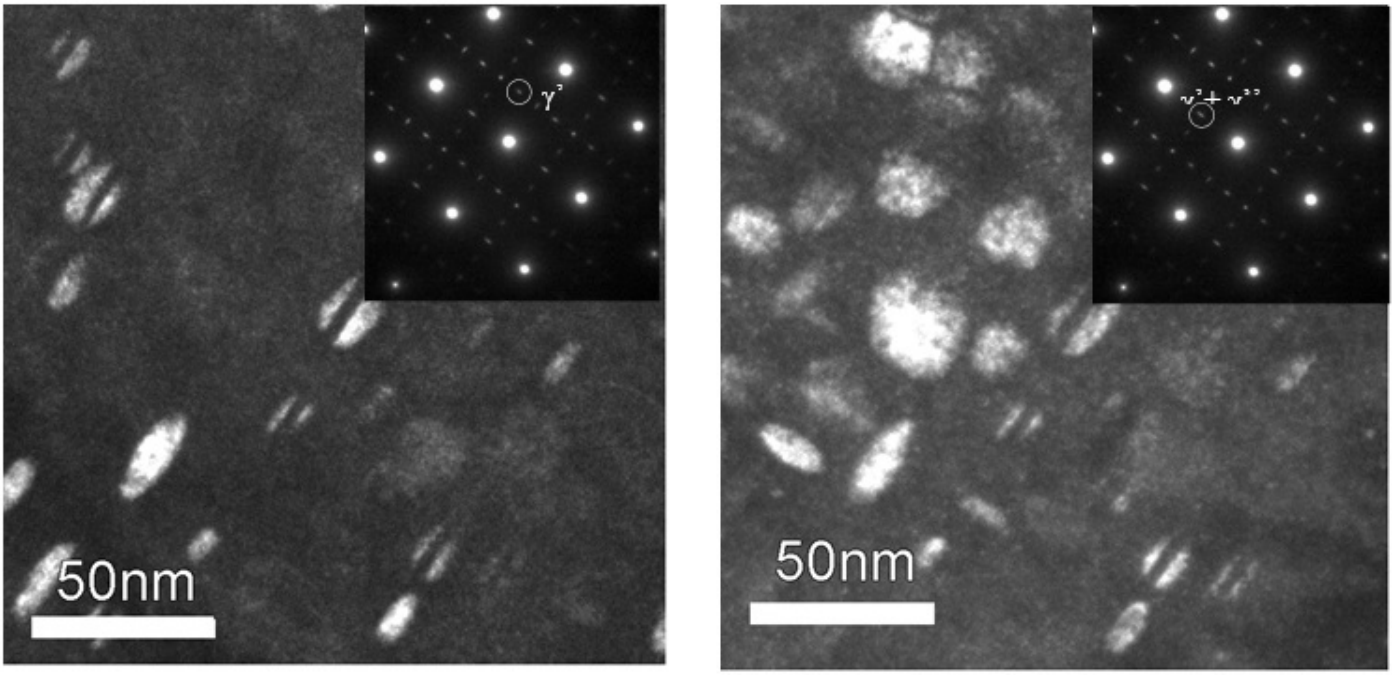


**Fig.6** - Precipitates characterization in AF955® Gr. 3HS. DF micrographs: (a) with only γ′′ SAD reflections showing elongated γ′′ precipitates; (b) with γ′ + γ′′ SAD reflections showing elongated γ′′ particles and cubical γ′ precipitates.

Mean long axis a and short axis c of elongated γ′′ precipitates and mean diameter d of γ′ precipitates were found out by image analysis of DF micrographs. The thicknesses t of the thin foils containing γ′′ and γ′ phases were evaluated by CBED method, so the volume fractions were calculated. The results of precipitates dimensions and volume fractions are reported in Table 5. In the Gr. 3HS, there was the presence of γ′ and γ′′ precipitates, whilst the γ′ phase was not detectable in the Gr. 3 sample. The volume fractions for γ′′ phase were similar in both the samples, with a slightly higher value for the Gr. 3 condition. For detailed calculations see [14].

**Tab.5** - Mean dimensions and volume fractions of γ'' and γ' precipitates in AF955® after different heat treatments as determined from the analysis of DF TEM micrographs. FV, γ' is he volume fraction of γ' precipitates and FV, γ'' of γ'' precipitates.

| | | | |
|---|---|---|---|
| **Gr. 3** | γ'' | a = 14.3 ± 3.0 nm<br>c = 6.7 ± 2.0 nm | $FV_{,\gamma''}$ =0.08 ± 0.02 |
| **Gr. 3HS** | γ'' | a = 15.2 ± 3.0 nm<br>c = 6.5 ± 2.0 nm | $FV_{,\gamma''}$ =0.06 ± 0.02 |
| | γ' | d = 13.5 ± 3 nm | $FV_{,\gamma''}$ =0.12 ± 0.02 |

According to the data gathered in Table 5, the inter-particle distances for Gr. 3 and Gr. 3HS were calculated. The Ashby-Orowan equation [15] defines the inter-particle distance λ as

$$\lambda = \frac{2r}{0.538 \cdot F_v^{1/2} \ln(2r/b)} \qquad 1)$$

where $r$ is the precipitate radius, and $b$ is the Burgers vector intensity. Since γ'' precipitates are oblate, an equivalent radius $r = (a^2c)^{1/3}$ was used as input in Eq. 1, and because of oblateness, λ in Eq. 1 has to be modified according to [16]

$$\lambda_{\gamma''} = h^{1/6}\left(\frac{2+h^2}{3}\right)^{-1/4} \cdot \lambda \qquad 2)$$

with $h = c/a$. In order to find the mean interparticles in Gr. 3HS distance because of γ'' and γ', the two mean inter-particle distances were summed according to [17]

$$\frac{1}{\lambda_{\gamma''+\gamma'}} = \frac{1}{\lambda_{\gamma''}} + \frac{1}{\lambda_{\gamma'}} \qquad 3)$$

In Table 6 the results of λ calculations are reported.

**Tab.6** - Mean inter-particle distances λ in AF955® after different heat treatments.

| | **Precipitates** | λ (nm) |
|---|---|---|
| **Gr. 3** | γ'' | 18.3 |
| **Gr. 3HS** | γ' + γ'' | 9.8 |

## DISCUSSION

### *Microstructure and mechanical properties*

The microstructure of metallic alloys resulting from thermo-mechanical processing like forging can results in significant microstructure and mechanical properties heterogeneity. The deformation through the workpiece from the surface to the core is heterogeneous because of external stress conditions and lubricant setting between workpiece and tools [12,13]. This heterogeneity can drive a heterogeneous evolution of the microstructure during deformation steps at high temperatures because of dynamic and meta-dynamic recrystallization, and also in subsequent heat treatments because of static recrystallization and grain growth. Therefore, mechanical properties can be significant heterogeneous with application problems in components. So, homogeneity has indeed to be obtained. In the production of 127 mm diameter bars of alloy AF955®, the grain size was homogeneous over the entire cross section and, consistently, the HRC hardness did not change significantly from the surface to the core of the bars.

The micrometric coarse precipitations resulted to be Nb(-Ti)C and Ti(Nb)N. These precipitations have no effects on the strength of nickel-base superalloy, since the antiparticle distance is by far larger than the Burgers vector length. However, they can affect the ductility of alloys particularly at high temperature, nucleating cracks and giving rise to premature

failures [15]. The heat treatment for the Gr. 3 produced a significant increase of strength (+129.7% of SY and +42.5% of UTS) and reduction of ductility (-41.3% of eR) compared to the alloy in S.A. conditions. The additional heat treatment at 621°C for 8 hours, followed by air cooling, for Gr. 3HS produced a higher increase of strength (+164.8% of SY and +55.3% of UTS) and larger reduction of ductility (-49.2% of eR). So, Gr. 3HS had a significant increase of strength with a little reduction of ductility compared to Gr. 3, and the more significant presence of coarse precipitates of carbides and nitrides did not seem to affect the ductility of Gr. 3HS at room temperature. Indeed, to have a further support to the rationalization of the effects of coarse precipitates on ductility and correlation between plastic deformation properties and microstructure, the strain hardening analysis has to be carried out according to the Kocks-Mecking approach [16-20]. In Fig. 7a the true stress-true strain curves of AF955® in S.A., Gr.3 and Gr. 3HS conditions are reported, where true stress $\boldsymbol{\sigma} = S\cdot(1 + e)$ and $\varepsilon = ln(1 + e)$ and $S$ and $e$ have the usual meaning. In Fig. 7b the strain hardening rate $d\boldsymbol{\sigma}/d\varepsilon$ is plotted against the true stress $\boldsymbol{\sigma}$. The line through the origin identify the Considére's criterion, $\Theta$ (= $d\boldsymbol{\sigma}/d\varepsilon$) = $\boldsymbol{\sigma}$, which identify the beginning of necking, i.e. the strain localization. All the tensile tests achieved the Considére's criterion, and run farther, indicating that no premature failures occurred.

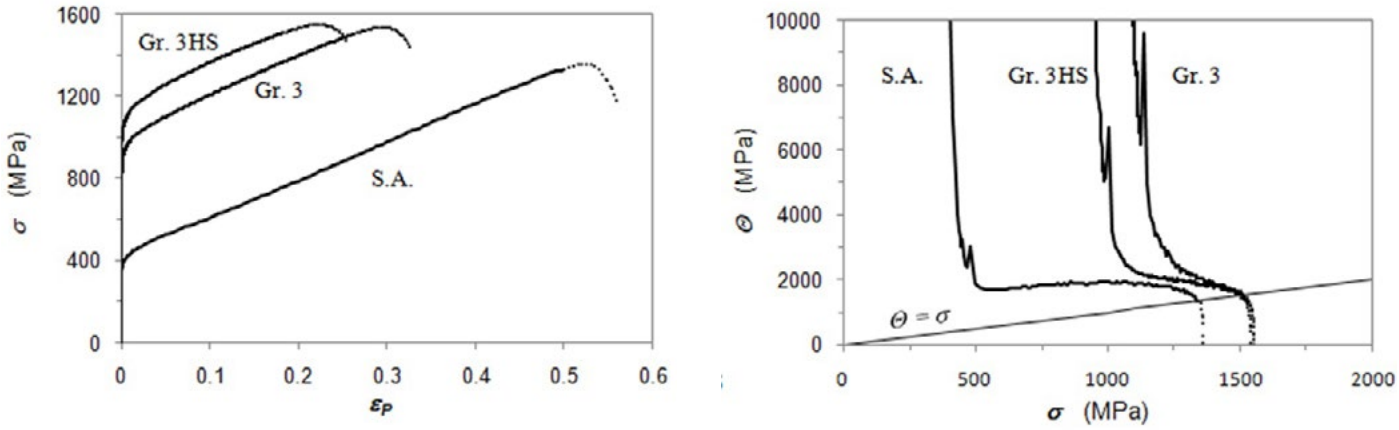


**Fig.7** - a) True stress-true strain flow curves of AF955® after solution annealing (S.A.), and heat treatments Gr. 3 and Gr. 3HS; b) Kocks-Mecking diagram: strain hardening data $\Theta$ (= $d\boldsymbol{\sigma}/d\varepsilon$) vs. $\boldsymbol{\sigma}$ of the flow curves in Fig. 7a. The line through the origin identify the Considére's criterion, $\Theta = \boldsymbol{\sigma}$, that is, the begin of strain localization.

***Correlation between yield stress and microstructure***

The significant increase of strength in metallic alloys occurs because of nanometric precipitates that have dimensions and characteristic inter-particle distances comparable to the Burgers vector modulus of λ matrix. So γ′ and γ′′ phase precipitates produced in AF955® after proper heat treatments contributed significantly to the strength increase. The flow stress of metallic alloys comes into two components [17]:

$$\sigma = \sigma_{Yield} + \sigma(\varepsilon_p) \qquad 4)$$

where $\boldsymbol{\sigma}_{Yield}$ is the yield strength in true stress, whilst $\boldsymbol{\sigma}(\varepsilon_p)$ is the true stress component because of the increase of dislocation density $\rho$ during straining. In AF955® strengthening occurs by solid solution in the γ matrix because of alloying elements and by precipitation hardening because of the phases γ′′ and γ′, so, through assuming that the initial dislocation density can be neglected, $\boldsymbol{\sigma}_{Yield}$ can be described as [22,23]

$$\sigma_{Yield} = \sigma_{SS} + \sigma_{PH} \qquad 5)$$

where $\boldsymbol{\sigma}_{SS}$ and $\boldsymbol{\sigma}_{PH}$ are the solid solution and the precipitation hardening stress components, respectively. For lower strains significant errors in the determination of $\boldsymbol{\sigma}_{Yield}$ could be introduced by the uncertainty in the experimental determinations of the Young modulus E, whilst at higher strains significant strain hardening was already established. So, values of flow stress at $\varepsilon_p$ = 0.1% were assumed as $\boldsymbol{\sigma}_{Yield}$, since $\varepsilon_p$ = 0.1% seemed to be a suitable compromise. So $\boldsymbol{\sigma}_{Yield}$ of the S.A. AF955® was found to be 383.2 MPa, while 879.8 MPa for Gr.3 and 1022.2 MPa for Gr. 3HS.

γ′ and γ′′ precipitates are deformable, that is, they are cut by mobile dislocations $a$/2<1-10>{111} gliding in the γ ma-

trix, so $\sigma_{PH}$ in Eq. 5 results in contributions from dfferent strengthening mechanisms resulting from cutting. Since γ′ and γ′′ phases are coherent to the γ matrix, misfit strain is present. Furthermore, and γ′ and γ′′ phases have crystallographic structures different from γ, antiphase boundaries (APB) are produced in the particles with cutting, and a second trailing coupled dislocation has to cut the particle again to erase the APB and set back the original crystallographic order. Therefore, the different hardening mechanisms involved in cutting coherent particles are as follows: first, the overcoming of the strain misfit between the coherent particle and the matrix, giving rise to an extra critical resolved shear stress $\sigma_{Coh}$; second, APB formation in the particle, producing σAPB; then, a chemical hardening due to the increase of the interface between the cut particle and the matrix, producing $\sigma_{Chem}$; and finally, a modulus hardening due to different shear moduli between the particle and the matrix, producing $\sigma_{Mod}$. Detailed equations are reported in [14,15,22,23]. Two possible rationalizations of APB strengthening can be given: Weakly Coupled Dislocations (WCD) model, when the coupling between leading and trailing dislocations cutting through the γ′ and γ′′ precipitates is weak (i.e. the distance between leading and trailing dislocations is larger than the mean precipitate size); and Strongly Coupled Dislocations (SCD) model, when the coupling between leading and trailing dislocations cutting through the γ′ and γ′′ precipitates is strong (i.e. die stance between leading and trailing dislocations is shorter than the mean precipitate size) [5,22,23]. In [22], these mechanisms are superimposed according to

$$\sigma_{PH} = \left(\sigma_{Coh}^{n} + \sigma_{APB}^{n} + \sigma_{Chem}^{n} + \sigma_{Mod}^{n}\right)^{1/n} \quad 6)$$

with $n$ = 1.8. Through using at $\sigma_{SS}$ = 383.2 MPa (stress for S.A. AF955® at $\varepsilon_p$ = 0.1%), the predictions of the yield stresses with Eq. 5 for AF955® Gr. 3 and Gr. 3HS for the WCD and SCD models [14] are reported in Table 7, for comparison. The yield stresses predicted by WCD model is closer to the experimental values of yield stresses. Indeed, the contributions from APB formation was dominant, in agreement with detailed simulations on the microstructure and strength evolution in the heat-treated superalloy 718 (UNS N07718) hardened by γ′′ and γ′ precipitation [16]. So, AF955® Gr. 3 resulted to be significantly strengthened by deformable γ′′ particles only, whilst Gr. 3HS resulted stronger than Gr. 3 because of the presence of deformable γ′′ and γ′ particles in a higher total volume fraction.

**Tab.7** - Comparison between experimental yield stresses $\sigma_{Y,Exp}$ and prediction from deformable particles for WCD and SCD models. The values $\sigma_{Y,Exp}$ were measured at $\varepsilon_p$ = 0.1% in AF955®.

| | σY,Exp(MPa) | σY,WCD(MPa) | σY,SCD(MPa) |
|---|---|---|---|
| **Gr. 3** | 879.8 | 944.0 ± 62.3 | 779.9 ± 46.1 |
| **Gr. 3HS** | 1022.2 | 1027.5 ± 78.5 | 895.8 ± 67.1 |

## CONCLUSIONS

The mechanical and strain hardening behavior of the new nickel-base superalloy AF955® after forging and two different heat treatments were investigated. Microstructure by OM and SEM and mechanical properties by Rockwell hardness and tensile testing were investigated in 127 mm diameters bars. The microstructure and mechanical homogeneity were investigated. The strain hardening analysis through Kocks-Mecking diagram confirmed good integrity as both Gr. 3 and Gr. 3HS achieved necking. For detailed rationalization of the response of the AF955® to different heat treatments, the dimensions and volume fractions of γ′′ and γ′ particles were quantified through TEM to rationalize the different mechanical behaviors. The Weakly Coupled Dislocations(WCD) model could explain quantitatively the precipitation hardening effects on the tensile mechancial properties AF955® after different heat treatments. AF955® Gr. 3 resulted to be significantly strengthened by deformable γ′′ particles only, whilst Gr. 3HS resulted stronger than Gr. 3 because of the presence of deformable γ′′ and γ′ particles in a higher total volume fraction.

## ACKNOWLEDGEMENTS

Mr. T. Ranucci and D. Della Torre from ICMATE-CNR are thanked for the technical support.

## REFERENCES

[1] B.F. Dyson, M. McLean, in: S. Murakami, N. Ohno (Eds.), Creep in Structures, Kluver Academic Publishers, The Netherlands, 2001.

[2] M. Maldini, V. Lupinc, G. Angella, Creep softening and strengthening mechanisms due to γ' raft development in SMP 14 single crystal nickel base superalloy at 1000°C, Kov. Mater.-Metallic Mater., 42 (2004) 21-30.

[3] M. Maldini, G. Angella, V. Lupinc, Analysis of creep curves of a nickel base superalloy in a wide stress/temperature range, Mater. Sci. Eng. A, 462 (2007) 436-440.

[4] B.D. Craig and L. Smith,Corrosion Resistant Alloys (CRAs) in the Oil and Gas Industry - Selection Guide Update, Nickel Inst. Tech. Ser., 2011, No. 10073.

[5] L. Popoola, A. Grema, G. Latinwo, B. Gutti, and A. Balogun, Corrosion problems during oil and gas production and its mitigation,Int. J. Ind. Chem.(2013)4:35.

[6] NACE MR0175/ISO 15156-3: 2009 (Second edition), Petroleum and natural gas industries – material for use in H2S-containing environments in oil and gas production – Part 3: Cracking-resistant CRAs (corrosion resistant alloys) and other alloys (Houston, TX: NACE International).

[7] L. Foroni, C. Malara, R. Montani and S. Gregory, UNS N09955: A new Ni-base alloy for H2S and hydrogen charging environments. CORROSION 2015, paper n. 5502 (Houston, TX: NACE International, 2015).

[8] L. Foroni, C. Malara, R. Montani and S. Gregory, UNS N09955 Corrosion Cracking Resistance, CORROSION 2016, paper n. 7355 (Vancouver, BC, Canada: NACE International 2016).

[9] API Standard 6ACRA – First Edition, Age-Hardened Nickel-Based Alloys for Oil and Gas Drilling and Production Equipment (Washington D.C., NW: API Publishing Services).

[10] B. Dubiel, A. Kruk, E. Stepniowska, G. Cempura, D. Geiger, P. Formanek, J. Hernandez, P. Midgley, and a Czyrska-Filemonowicz, TEM, HRTEM, electron holography and electron tomography studies of γ′ and γ′′ nanoparticles in Inconel 718 superalloy, J. Microsc., 236 (2009) 149–57.

[11] K. Kulawik, P.A. Buffat, A. Kruk, A.M. Wusatowska-Sarnek, and A. Czyrska-Filemonowicz, maging and characterization of γ′ and γ′ nanoparticles in Inconel 718 by EDX elemental mapping and FIB–SEM tomography,Mater. Charact., 100 (2015) 74–80.

[12] Chamanfar, A., Sarrat, L., Jahazi, M., Asadi, M., Weck, A., Koul, A.K., Microstructural characteristics of forged and heat treated Inconel-718 disks, Mat and Design, 52 (2013) 791-800.

[13] Gupta, C., Jha, J.S., Jayabalan, B., Alankar, A., Mishra, S., Correlating Hot Deformation Parameters with Microstructure Evolution During Thermo-mechanical Processing of Inconel 718 Alloy, Metall Mater Trans A, 50 (2019) 4714-4731.

[14] A, Serafini, G. Angella, C. Malara, M.F. .Brunella: Mechanical and Microstructural Characterization of AF955® (UNS N09955) Nickel-Based Superalloy After Different Heat Treatments, Metall Mater Trans A, 49 (2018). 5339-5352

[15] C. Reed: The superalloys, Fundamentals and Applications, Cambridge University Press, 2006.

[16] M R Ahmadi, M Rath, E Povoden-Karadeniz, S Primig, T Wojcik, A Danninger, M Stockinger, E Kozeschnik, Modeling of precipitation strengthening in Inconel 718 including non-spherical γ'' precipitates, Model. Simul. Mater. Sci. Eng.A, 25 (2017) 055005(16pp)

[17] U.F. Kocks, H. Mecking, Physics and phenomenology of strain hardening: the FCC case, Prog. Mater. Sci., 48 (2003) 171-273.

[18] G. Angella, B.P. Wynne, W.M. Rainforth, J.H. Beynon, Strength of AISI 316L in torsion at high temperature, Mater. Sci. Eng. A, 475 (2008) 257-267.

[19] G. Angella, R. Donnini, M. Maldini, D. Ripamonti, Combination between Voce formalism and improved Kocks-Mecking approach to model small strains of flow curves at high temperatures, Mater. Sci. Eng. A, 594 (2014) 381-388.

[20] K.V.U. Praveen, G.V.S. Sastry, V. Singh, Work-hardening behavior of the Ni-Fe based superalloy IN718,Metall. Mater. Trans. A, 39 (2008) 65-78.

[21] Shaik Khaja, K.K. Mehta, R. Veera Babu, S. Sri Rama Devi, A.K. Singh, Mechanical Properties Anisotropy of Isothermally Forged and Precipitation Hardened Inconel 718 Disk, Metall. Mater. Trans. A, 46 (2015) 1140-1153.

[22] A.J. Ardell, Precipitation Hardening, Metall. Trans., 16 (1985) 2131-2165.

[23] R. Schnitzer, S. Zinner, H. Leitner, Modeling of the yield strength of a stainless maraging steel, Scr. Mater, 62 (2010) 286-289.